Applied Physics Letters

Ultrathin interfacial layer with suppressed room temperature magnetization in magnesium aluminum ferrite thin films

Cite as: Appl. Phys. Lett. **115**, 132404 (2019); https://doi.org/10.1063/1.5111326
Submitted: 28 May 2019 . Accepted: 06 September 2019 . Published Online: 24 September 2019

Jacob J. Wisser, Satoru Emori, Lauren Riddiford, Aaron Altman, Peng Li, Krishnamurthy Mahalingam, Brittany T. Urwin, Brandon M. Howe, Michael R. Page, Alexander J. Grutter, Brian J. Kirby, and Yuri Suzuki

Applied Physics Letters ARTICLE scitation.org/journal/apl

Ultrathin interfacial layer with suppressed room temperature magnetization in magnesium aluminum ferrite thin films

Cite as: Appl. Phys. Lett. **115**, 132404 (2019); doi: 10.1063/1.5111326
Submitted: 28 May 2019 · Accepted: 6 September 2019 ·
Published Online: 24 September 2019

View Online Export Citation CrossMark

Jacob J. Wisser,[1,a)] Satoru Emori,[2] Lauren Riddiford,[1] Aaron Altman,[3] Peng Li,[4] Krishnamurthy Mahalingam,[5] Brittany T. Urwin,[5] Brandon M. Howe,[5] Michael R. Page,[5] Alexander J. Grutter,[6] Brian J. Kirby,[6] and Yuri Suzuki[1]

AFFILIATIONS

[1]Department of Applied Physics, Stanford University, Stanford, California 94305, USA
[2]Department of Physics, Virginia Tech, Blacksburg, Virginia 24061, USA
[3]Department of Mathematics, Stanford University, Stanford, California 94305, USA
[4]Geballe Laboratory for Advanced Materials, Stanford University, Stanford, California 94305, USA
[5]Materials and Manufacturing Directorate, Air Force Research Laboratory, Wright-Patterson Air Force Base, Dayton, Ohio 45433, USA
[6]NIST Center for Neutron Research, National Institute of Standards and Technology, Gaithersburg, Maryland 20899, USA

[a)]jwisser@stanford.edu

ABSTRACT

Low-damping magnetic oxide thin films with small thicknesses are essential for efficient insulator spintronic devices, particularly those driven by spin torque effects. Here, we investigate the depth-resolved compositional and magnetic properties of epitaxial spinel $MgAl_{0.5}Fe_{1.5}O_4$ (MAFO), which has recently been reported as a promising low-damping insulator. We find that ≈11 nm films exhibit optimal Gilbert damping, with a typical damping parameter of 0.001. While defects due to strain relaxation in the bulk of the film contribute to increased damping for large film thickness, the damping increase in thinner films is attributed to the presence of a chemically disordered magnetic dead layer at the film/substrate interface. This interfacial dead layer arises from an Fe-deficient MAFO layer. Notably, this layer is only about one-sixth the thickness of that found at the interface between yttrium iron garnet films and gadolinium gallium garnet substrates, making MAFO an ideal thin-film insulator for spin-torque applications.

Spintronics has largely been based on the control of spin-polarized charge current, but recently magnetic insulators driven by pure spin current (without any charge current) have been recognized as more energy-efficient media for spintronics.[1,2] The most oft-studied magnetic insulator is yttrium iron garnet (YIG) grown on gadolinium gallium garnet (GGG), which boasts a typical magnetic damping parameter of $\alpha_{eff} \approx 0.0001-0.001$.[3–13] However, some properties of YIG are not ideal for future applications. Epitaxial YIG films with low damping require high temperatures (≈750 °C) for crystallization during growth or postannealing, which is not ideal for minimizing the thermal budget for large scale integration.[3–13] Furthermore, the high processing temperature promotes atomic interdiffusion, e.g., of Gd into the YIG film, resulting in an ≈5–6 nm-thick magnetic dead layer at the YIG/GGG interface, which may suppress the Curie temperature and cause an undesirable increase in damping for very thin YIG films.[13–15] This disordered layer can be problematic for driving precessional magnetization dynamics in YIG with spin-torque effects, which require both low damping and small magnetic thickness.[5,16–20] Therefore, the ability to realize ultrathin low-loss magnetic insulator films is crucial to the success of pure-spin-current-based spintronics.

As an alternative to YIG films, we have recently synthesized epitaxial spinel-ferrite thin films of $MgAl_{0.5}Fe_{1.5}O_4$ (MAFO) grown on $MgAl_2O_4$ (MAO) substrates. MAFO films between 10 and 15 nm thick exhibit a very low Gilbert damping parameter on the order of YIG films ($\alpha_{MAFO} \approx 0.001$),[21] and spin pumping has been demonstrated from MAFO films into the canonical spin sinks Pt and β-W.[22] MAFO films crystallize at significantly lower temperatures than YIG, such that the problem of interfacial interdiffusion may be reduced.

Additionally, the substrate MAO is diamagnetic at all temperatures, greatly diminishing the substrate contribution to magnetic measurements. More importantly, the effective magnetization of MAFO is significantly higher than YIG, resulting in significantly reduced external field requirements for ferromagnetic resonance.[21,23,24] The spinel crystal structure also offers more opportunities for integration with other oxide materials and silicon.[25–28] Similar to YIG/GGG systems, MAFO/MAO exhibits a degradation of the saturation magnetization and Gilbert damping in the ultrathin regime ($t < 10$ nm),[21] pointing to the possible existence of an interfacial layer at the film/substrate interface and the film surface.

In this paper, we study the magnetic response of MAFO films grown on MAO substrates as a function of thickness in order to determine the factors limiting magnetic damping. Through x-ray reflectivity (XRR), superconducting quantum interference device (SQUID) magnetometry, and magnetic depth profiling performed via polarized neutron reflectometry (PNR), we have determined that there is a magnetically suppressed layer ≈1.025 nm thick at the film/substrate interface. This layer is nearly one-sixth of the thickness found in YIG/GGG systems and a little over one spinel structure unit cell. The presence of this layer is enough to substantially increase the Gilbert damping parameter in ultrathin MAFO films but is negligible in thicker ($t > 10$ nm) MAFO films. In thicker MAFO films, defects associated with plastic deformation contribute to an increased Gilbert damping.

All films were grown via pulsed laser deposition (PLD) on the as-received single-crystal (001) $MgAl_2O_4$ (MAO) substrates. MAO has a lattice constant of 8.08 Å, 3% smaller than MAFO, which has a bulk lattice constant of 8.30 Å, as determined by powder x-ray diffraction of the target. All films were deposited at a substrate temperature of 450 °C, under 10 mTorr (1.33 Pa) of oxygen pressure, and using a 248 nm KrF laser with a fluence of ≈1 J/cm^2. Samples were cooled under 100 Torr (13.3 Pa) of oxygen, and growth rates were calculated using x-ray reflectivity. The details of the deposition conditions have been published elsewhere.[21,22] X-ray diffraction studies indicate that thin ($t < 40$ nm) MAFO films are highly crystalline, exhibiting distinct Laue oscillations around the (004) Bragg reflection [see Fig. 1(a)]. A previous study has verified that MAFO films less than 40 nm thick are coherently strained to the MAO substrate via reciprocal space mapping of the $(\bar{1}\bar{1}5)$ reflection and transmission electron microscopy (TEM) imaging.[21] In thicker samples ($t > 40$ nm), Laue oscillations disappear as the film begins to relax to relieve the compressive strain induced by the lattice mismatch between the film and the substrate. We note that the calculated Matthews-Blakeslee critical thickness for relaxation and plastic deformation for MAFO on MAO is approximately 19 nm, which is consistent with our XRD data showing relaxation toward the bulk values of the out of plane lattice parameter of films thicker than 21 nm.[29] TEM results indicate that such a relaxation is accompanied by the formation of dislocations throughout the film, particularly at the film/substrate interface.[21] Additionally, energy dispersive spectroscopy (EDS) indicates that there is a layer at the film/substrate interface (see the supplementary material) in which the iron content is suppressed from the nominal film stoichiometry.

X-ray reflectivity (XRR) measurements were performed to calibrate the growth rate and investigate the film/substrate interface. Fits to XRR data were only successful when an interfacial layer was added to the model [see Fig. 1(b)]; a two-layer model comprised of a single layer film and a substrate gives a poor fit, as indicated by the blue fit curve in Fig. 1(b). Note that the fit deviates at a higher angle, owing to the fact that the model fails to take into account the interfacial region. Two-layer fits indicate that the interfacial region is about 1–2 nm with a density of ≈4.09 g/cm^2 (about 6% less dense than that of bulk MAFO as measured by XRR). Since the only difference between the film and substrate is the presence of iron, we postulate that this interfacial region consists of an iron-deficient composition of MAFO. This is consistent with the interfacial layer observed via EDS (see Fig. S1 in the supplementary material). The surface roughness measured by XRR is approximately 0.33 nm, which agrees well with the roughness measured via atomic force microscopy (AFM) of about 0.3 nm. The roughnesses measured via AFM and XRR do not show any systematic or significant trend with film thickness.

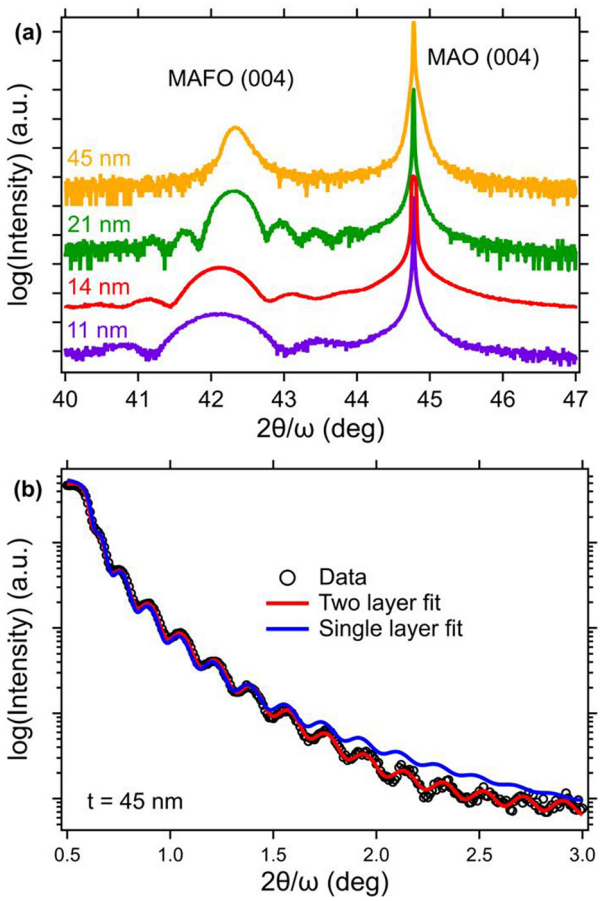

FIG. 1. (a) $2\theta - \omega$ XRD scans for different film thicknesses showing clear Laue oscillations. (b) XRR fitting of a 45 nm sample using a single-(blue) and a two-layer (red) model. The two-layer model includes a 1–2 nm interfacial layer of lower density than bulk MAFO and gives a much better fit.

To study the magnetic character of the interfacial region, we performed field dependent magnetization measurements as a function of MAFO film thickness. Films 5–21 nm thick exhibit very low coercivity ($H_c < 0.5$ mT), while thicker films have a marked increase in coercivity, with $H_c \approx 5$ mT for 45 nm films [as in Fig. 2(a)]. This increased coercivity in thicker films is correlated with an increased number of

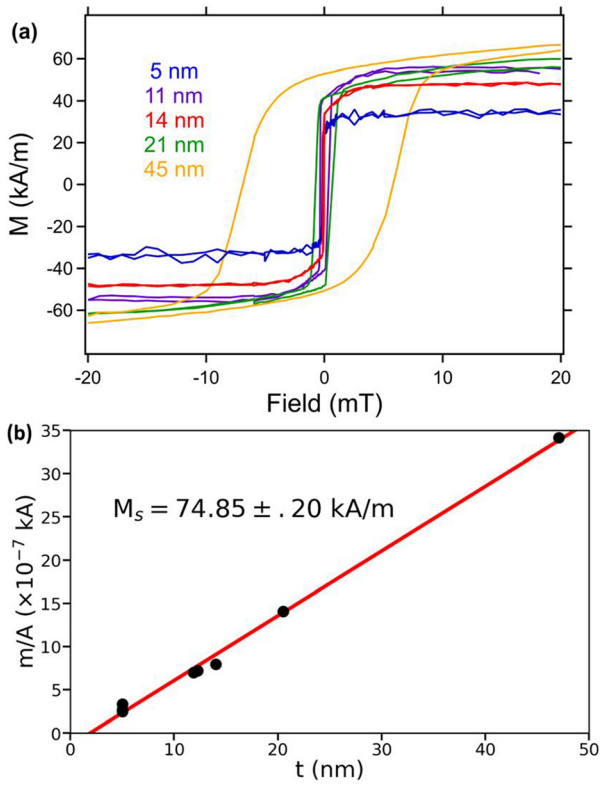

FIG. 2. (a) Magnetic hysteresis loops taken by SQUID magnetometry for different film thicknesses. Coercivity increases as the films relax at higher thicknesses. (b) Magnetic moment per area as a function of film thickness. Extrapolating to zero magnetic moment yields a 1.90 nm thick layer with zero magnetization.

defects which is associated with structural relaxation. Measuring the saturation moment per unit area as a function of thickness [see Fig. 2(b)], we observe a linear relationship with a slope corresponding to a constant saturation magnetization of $M_s = 74.85 \pm 0.20$ kA/m. Extrapolating the fit to zero magnetization, we have determined that these films exhibit an ≈1.90 ± 0.45 nm layer with zero magnetization (unless otherwise noted, uncertainties represent one standard deviation). While a similar layer has been proven to exist at the interface between YIG/GGG, SQUID magnetometry alone cannot provide information on the precise location of the layer—whether at the film/substrate interface or the film surface.

To directly characterize this layer in the system, polarized neutron reflectometry (PNR) was performed on the Polarized Beam Reflectometer (PBR) instrument at the NIST Center for Neutron Research. Measurements were performed at room temperature in applied in-plane fields of 7.5 mT and 600 mT. Incident neutrons were polarized to be spin up or down with respect to this field. The specular reflectivity of spin-polarized neutrons (which is dependent on the depth profile of the nuclear composition and of the sample magnetization component parallel to the applied field) is plotted as a function of wavevector transfer, Q, along the film normal [see Fig. 3(a)]. The sample magnetization is related to the splitting between the spin up and down reflectivities. This splitting is plotted as a spin asymmetry [Fig. 3(b)]

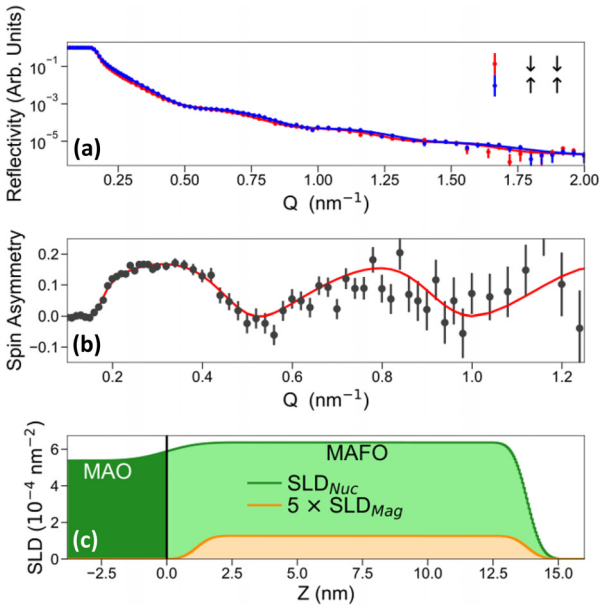

FIG. 3. (a) Neutron reflectivity data as a function of scattering wavevector, Q, with fits. (b) Calculated spin asymmetry fitted as a function of Q. (c) Nuclear and magnetic scattering length density profiles calculated using a three-layer model. Error bars represent one standard deviation.

which is calculated as the difference between the spin up and down reflectivities normalized by their sum. The fitting of the reflectivity data was carried out with the NIST Refl1D software package using a Markov-chain Monte Carlo algorithm for χ^2 optimization. We find that the magnetic depth profile is extremely well described by a model with a single magnetic layer of uniform magnetization and a thinner layer at the MAO/MAFO interface with zero magnetization. The resulting depth profiles at 7.5 mT are shown in Fig. 3(c), yielding a 1.025 ± 0.15 nm layer between the film and substrate with zero magnetization, in excellent agreement with the value of the intercept of the thickness axis in Fig. 2. We further note that the structural depth profile (described by the nuclear scattering length density) shows signs of interfacial intermixing found in the nuclear depth profile. The MAO/MAFO and MAFO/air interfaces exhibit roughnesses of 0.93 nm ± 0.05 nm and 0.44 nm ± 0.01 nm, respectively. The surface roughness observed by PNR is consistent with AFM and XRR measurements. The larger interface roughness observed by PNR at the MAO/MAFO interface likely indicates Fe diffusion. The dead layer we observe is slightly different from that in YIG/GGG systems, in that it does not form an antiparallel magnetic moment to the film magnetization and is much thinner. The lower degree of diffusion between the film and substrate is likely due to the lower crystallization/growth temperature of our spinel ferrite thin films (450 °C compared to ≈750 °C).

To characterize the dead layer's effect on spin current generation efficiency, we performed broadband ferromagnetic resonance (FMR) measurements at room temperature in a coplanar waveguide setup. For each measurement, the microwave frequency was fixed, while the magnetic field was swept and the derivative of the power absorption with respect to the field was measured via an rf diode. The resonant field, H_{FMR}, and linewidth, ΔH, were extracted from the FMR spectra.

The resonant field can be fit to the in-plane Kittel equation to yield the Landé g-factor and effective magnetization

$$f = \frac{g\mu_B}{h}\mu_0[(H_{FMR} + H_{4,\|})(H_{FMR} + M_{eff} + H_{4,\|})]^{1/2}, \quad (1)$$

where g is the Landé g-factor, μ_0 is the permeability of free space, μ_B is the Bohr magneton, h is Planck's constant, $H_{4,\|}$ is the in-plane cubic anisotropy field, and M_{eff} is the effective magnetization that accounts for the out-of-plane uniaxial anisotropy field. Fitting the resonant field as a function of frequency to the in-plane Kittel equation yields a Landé g-factor of ≈2.05, an in-plane cubic anisotropy field $|H_{4,\|}| \approx 6$ mT, and a remarkably large effective magnetization $\mu_0 M_{eff} \approx 1.5$ T which strongly prefers the moment to lie in the plane of the film. We did not observe any systematic change in the $H_{4,\|}$ parameter as a function of thickness, despite film relaxation. That $g \approx 2$ implies low spin–orbit coupling, as to be expected from the dominating Fe^{3+} contribution to the magnetic moment that has been confirmed by x-ray absorption spectroscopy.[21] Low spin–orbit coupling suppresses magnon-phonon scattering, leading to lower magnetic damping as discussed below.

Fitting the FMR linewidth ΔH as a function of frequency, f, to the in-plane Kittel equation yields the Gilbert damping parameter, α_{eff}

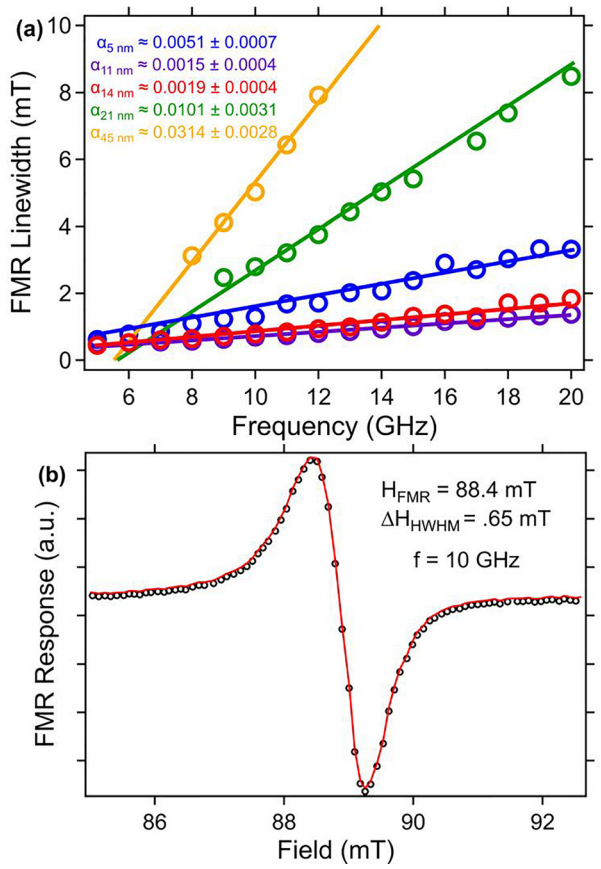

FIG. 4. (a) FMR ΔH vs frequency for MAFO films of various thicknesses. (b) Raw FMR data and fit for an 11 nm film measured at 10 GHz.

$$\Delta H = \Delta H_0 + \frac{h\alpha_{eff}}{g\mu_0\mu_B}f, \quad (2)$$

where ΔH_0 is the zero-frequency linewidth. Thin MAFO films (10 nm $< t_{MAFO} <$ 15 nm) exhibit a damping parameter of $\alpha_{eff} \approx 0.0015$ [Fig. 4(a)], which is almost an order of magnitude less than Permalloy and within the typically reported range for YIG/GGG films. In thicker MAFO films, the damping increases, with $\alpha_{eff} \approx 0.0314$ for 45 nm thick films. This has been attributed to the relaxation of the film and the formation of dislocations at higher thicknesses as discussed above. Thinner MAFO films also exhibit increased damping, with $\alpha_{eff} \approx 0.0051$ for 5 nm films. The mechanism for this increased damping is now understood to be the dominance of the interfacial layer in thinner films. If the dead layer is indeed an iron-deficient composition of MAFO with degraded magnetic properties, then we would expect an increase in the Gilbert damping in the thinnest films as the dead layer plays an increasingly larger role in the magnetic properties of the film. In thicker films (10–14 nm thickness range), it is not yet energetically favorable for the film to undergo plastic deformation. In these coherently strained films, the dead layer plays an increasingly smaller role in the magnetic properties and Gilbert damping can be minimized.

We have demonstrated that epitaxial MAFO films grown on MAO substrates exhibit an interfacial layer with zero magnetization approximately 1.025 nm thick. XRR, SQUID magnetometry, and PNR provide a comprehensive magnetic profile of our MAFO films. The layer that we observe is nearly one-sixth the thickness of that observed in YIG/GGG systems, so that we are able to realize thinner low-loss ferromagnetic insulating films. This is promising for the realization of efficient spin-torque switching and miniaturization of devices in spin current based devices.

See the supplementary material for transmission electron microscopy images and x-ray energy dispersive spectroscopy measurements taken on a 14 nm film.

This work was supported by the U.S. Department of Energy, Director, Office of Science, Office of Basic Energy Sciences, Division of Materials Sciences and Engineering under Contract No. DESC0008505. L.R., A.A., and P.L. were funded by the Vannevar Bush Faculty Fellowship program sponsored by the Basic Research Office of the Assistant Secretary of Defense for Research and Engineering and funded by the Office of Naval Research through Grant No. N00014-15-1-0045. Part of this work was performed at the Stanford Nano Shared Facilities (SNSF), supported by the National Science Foundation under Award No. ECCS-1542152. X-ray diffraction was performed at the Stanford Nano Shared Facilities at Stanford University, supported by the National Science Foundation under Award No. ECCS-1542152. Transmission electron microscopy was performed at the Materials and Manufacturing Directorate at the Air Force Research Laboratory and was supported by the Air Force Office of Scientific Research under Project No. FA9550-15RXCOR198.

REFERENCES

[1]H. Adachi and S. Maekawa, "Spin waves, spin currents and spin Seebeck effect," in *Magnonics: From Fundamentals to Applications* (Springer Berlin Heidelberg, Berlin, Heidelberg, 2013), pp. 119–128.

[2]A. V. Chumak, V. Vasyuchka, A. Serga, and B. Hillebrands, Nat. Phys. **11**, 453 (2015).
[3]B. Heinrich, C. Burrowes, E. Montoya, B. Kardasz, E. Girt, Y.-Y. Song, Y. Sun, and M. Wu, Phys. Rev. Lett. **107**, 066604 (2011).
[4]C. Burrowes, B. Heinrich, B. Kardasz, E. A. Montoya, E. Girt, Y. Sun, Y.-Y. Song, and M. Wu, Appl. Phys. Lett. **100**, 092403 (2012).
[5]Y. Sun, Y.-Y. Song, H. Chang, M. Kabatek, M. Jantz, W. Schneider, M. Wu, H. Schultheiss, and A. Hoffmann, Appl. Phys. Lett. **101**, 152405 (2012).
[6]M. Collet, X. de Milly, O. d'Allivy Kelly, V. V. Naletov, R. Bernard, P. Bortolotti, J. Ben Youssef, V. E. Demidov, S. O. Demokritov, J. L. Prieto, M. Muñoz, V. Cros, A. Anane, G. de Loubens, and O. Klein, Nat. Commun. **7**, 10377 (2016).
[7]C. Hahn, G. de Loubens, O. Klein, M. Viret, V. V. Naletov, and J. Ben Youssef, Phys. Rev. B **87**, 174417 (2013).
[8]M. B. Jungfleisch, A. V. Chumak, A. Kehlberger, V. Lauer, D. H. Kim, M. C. Onbasli, C. A. Ross, M. Kläui, and B. Hillebrands, Phys. Rev. B **91**, 134407 (2015).
[9]Y. Sun, H. Chang, M. Kabatek, Y.-Y. Song, Z. Wang, M. Jantz, W. Schneider, M. Wu, E. Montoya, B. Kardasz, B. Heinrich, S. G. E. te Velthuis, H. Schultheiss, and A. Hoffmann, Phys. Rev. Lett. **111**, 106601 (2013).
[10]T. Liu, H. Chang, V. Vlaminck, Y. Sun, M. Kabatek, A. Hoffmann, L. Deng, and M. Wu, J. Appl. Phys. **115**, 17A501 (2014).
[11]H. Kurebayashi, O. Dzyapko, V. E. Demidov, D. Fang, A. J. Ferguson, and S. O. Demokritov, Nat. Mater. **10**, 660 (2011).
[12]P. Pirro, T. Brächer, A. V. Chumak, B. Lägel, C. Dubs, O. Surzhenko, P. Görnert, B. Leven, and B. Hillebrands, Appl. Phys. Lett. **104**, 012402 (2014).
[13]M. C. Onbasli, A. Kehlberger, D. H. Kim, G. Jakob, M. Kläui, A. V. Chumak, B. Hillebrands, and C. A. Ross, APL Mater. **2**, 106102 (2014).
[14]A. Mitra, O. Cespedes, Q. Ramasse, M. Ali, S. Marmion, M. Ward, R. M. D. Brydson, C. J. Kinane, J. F. K. Cooper, S. Langridge, and B. J. Hickey, Sci. Rep. **7**, 11774 (2017).
[15]J. F. K. Cooper, C. J. Kinane, S. Langridge, M. Ali, B. J. Hickey, T. Niizeki, K. Uchida, E. Saitoh, H. Ambaye, and A. Glavic, Phys. Rev. B **96**, 104404 (2017).
[16]O. d'Allivy Kelly, A. Anane, R. Bernard, J. Ben Youssef, C. Hahn, A. H. Molpeceres, C. Carrétéro, E. Jacquet, C. Deranlot, P. Bortolotti, R. Lebourgeois, J.-C. Mage, G. de Loubens, O. Klein, V. Cros, and A. Fert, Appl. Phys. Lett. **103**, 082408 (2013).
[17]M. Jungfleisch, W. Zhang, J. Sklenar, J. Ding, W. Jiang, H. Chang, F. Fradin, J. Pearson, J. Ketterson, V. Novosad, M. Wu, and A. Hoffmann, Phys. Rev. Lett. **116**, 057601 (2016).
[18]C. Safranski, I. Barsukov, H. K. Lee, T. Schneider, A. A. Jara, A. Smith, H. Chang, K. Lenz, J. Lindner, Y. Tserkovnyak, M. Wu, and I. N. Krivorotov, Nat. Commun. **8**, 117 (2017).
[19]O. V. Prokopenko, I. N. Krivorotov, T. J. Meitzler, E. Bankowski, V. S. Tiberkevich, and A. N. Slavin, in *2013 International Kharkov Symposium on Physics and Engineering of Microwaves, Millimeter and Submillimeter Waves* (IEEE, 2013), pp. 143–161.
[20]C. O. Avci, A. Quindeau, C.-F. Pai, M. Mann, L. Caretta, A. S. Tang, M. C. Onbasli, C. A. Ross, and G. S. D. Beach, Nat. Mater. **16**, 309 (2017).
[21]S. Emori, D. Yi, S. Crossley, J. J. Wisser, P. P. Balakrishnan, B. Khodadadi, P. Shafer, C. Klewe, A. T. N'Diaye, B. T. Urwin, K. Mahalingam, B. M. Howe, H. Y. Hwang, E. Arenholz, and Y. Suzuki, Nano Lett. **18**, 4273 (2018).
[22]L. Riddiford, J. Wisser, S. Emori, P. Li, D. Roy, E. Cogulu, O. Erve, Y. Deng, S. Wang, B. Yonker, A. Kent, and Y. Suzuki, "Efficient spin current generation in low-damping $Mg(Al,Fe)_2O_4$ thin films," Appl. Phys. Lett. (unpublished).
[23]M. Gray, S. Emori, B. Gray, H. Jeon, O. van 't Erve, B. Jonker, S. Kim, M. Suzuki, T. Ono, B. Howe, and Y. Suzuki, Phys. Rev. Appl. **9**, 064039 (2018).
[24]S. Emori, B. A. Gray, H.-M. Jeon, J. Peoples, M. Schmitt, K. Mahalingam, M. Hill, M. E. McConney, M. T. Gray, U. S. Alaan, A. C. Bornstein, P. Shafer, A. T. N'Diaye, E. Arenholz, G. Haugstad, K.-Y. Meng, F. Yang, D. Li, S. Mahat, D. G. Cahill, P. Dhagat, A. Jander, N. X. Sun, Y. Suzuki, and B. M. Howe, Adv. Mater. **29**, 1701130 (2017).
[25]L. M. B. Alldredge, R. V. Chopdekar, B. B. Nelson-Cheeseman, and Y. Suzuki, Appl. Phys. Lett. **89**, 182504 (2006).
[26]N. Wakiya, S. Sawamura, K. Tanemura, M. Sano, N. Sakamoto, D. Fu, K. Shinozaki, and H. Suzuki, Jpn. J. Appl. Phys. **48**, 09KB06 (2009).
[27]J. M. Iwata-Harms, R. V. Chopdekar, F. J. Wong, B. B. Nelson-Cheeseman, C. A. Jenkins, E. Arenholz, and Y. Suzuki, Appl. Phys. Lett. **106**, 012405 (2015).
[28]S.-B. Mi, C.-L. Jia, V. Vaithyanathan, L. Houben, J. Schubert, D. G. Schlom, and K. Urban, Appl. Phys. Lett. **93**, 101913 (2008).
[29]J. Matthews, A. Blakeslee, and S. Mader, Thin Solid Films **33**, 253 (1976).